THE INTENSITY, VELOCITY AND MAGNETIC STRUCTURE OF A SUNSPOT REGION

IV: *Properties of a Unipolar Sunspot*

J. M. BECKERS

Sacramento Peak Observatory, Air Force Cambridge Research Laboratories, Sunspot, N.M., U.S.A.

and

E. H. SCHRÖTER

Universitäts-Sternwarte, Göttingen, Germany

(Received 3 July, 1969)

Abstract. From an investigation of spectra in a magnetically sensitive ($\lambda 6173$, $g = 2.5$) and insensitive line ($\lambda 5576$, $g = 0$), we derived the following properties for a symmetrical sunspot:

(a) The magnetic field strength varies with the distance $\varrho (\varrho \leqslant 1)$ from the sunspot center like $H(\varrho) = H(0)\,(1 + \varrho^2)^{-1}$.

(b) The zenith angle of the magnetic field varies like $90^\circ \varrho$. From this and from $H(\varrho)$ we find a height gradient of 0.5 gs/km at $\varrho = 0$.

(c) The equivalent width and the half width of $\lambda 5576$ show an increase in penumbral regions of maximum Evershed flow. Most likely this is due to a combination of inhomogeneities in the Evershed flow and 'microturbulence'.

(d) We find the magnetic field strength to be larger in the dark interfilamentary regions of the penumbra. These regions move downwards with respect to the bright filaments and probably have a more horizontal magnetic field.

(e) In a weak light bridge and in extensions of bright penumbral filaments into the umbra, we find a decrease of the magnetic field strength, and a more horizontal field direction with respect to the umbral surrounding.

(f) In umbral dots and in the light bridge we find a relative upward motion.

1. Introduction

As part of a detailed study of a sunspot during its disk passage, we observed from 20 July 1966 to 1 August 1966 the sunspot numbered 4386 in the Rome monthly bulletin. Some results of these observations concerning the magnetic fields in the photosphere surrounding the spot and the properties of umbral dots have already been published (Beckers and Schröter, 1968a, b, c, 1969). In this publication we will describe the average magnetic and velocity field in this one sunspot as well as fluctuations in these fields associated with penumbral and umbral fine structures. Some of our results are a repetition of previous observations, but with a more refined reduction method. We also consider it to be important to know most physical quantities associated with this particular sunspot. Results concerning the center-to-limb variation of the intensity in different wavelengths and the Wilson effect in this specific sunspot will be published independently (Wittmann and Schröter, 1969; Wittmann, 1968; Wilson and McIntosh, 1969).

2. Observations and Reductions

Figure 1 in Beckers and Schröter (1968a) shows the setup used to obtain the sunspot spectra. In this paper one also finds detailed data about the sunspot under investigation. These spectra were taken simultaneously in the Fe line, 5576.1 Å line ($g=0$) and in the Fe line 6173.3 Å ($g=2.5$) in many positions across the sunspot. They were exposed for 10 sec at a rate of 15 sec. Simultaneously with the spectra we obtained slit-jaw images in integrated light and photoheliograms in blue and red continuous radiation. Often Hα filtergrams are also available. The diameter of the solar image for all observations equals 250 mm. Out of the many spectrograms (≈ 600) taken of the sunspot at different positions in the spot, we selected for each day 15–17 spectra of the best quality which covered all positions in and around the spot. These spectra were reduced by measuring the line profile of $\lambda 6173$ and $\lambda 5576$ at points 600 km apart with the Sacramento Peak automatically digitized microphotometer. At each point the 'Doppler line' ($\lambda 5576.1$) was scanned in a wavelength range of 0.9 Å centered on the line; the intensity readings were digitized every 7 mÅ. Intensity readings of each of the two 'Zeeman spectra' ($\lambda 6173.3$) corresponding to opposite circular polarizations were measured every 15.6 mÅ in an interval of 0.78 Å centered on the line. The resulting measurements were reduced by computer to give quantities like Doppler shift, equivalent width, Zeeman splitting, etc. The reduction was done with three different programs called, respectively, Doppler program (for Doppler line), and Zeeman 1 and 2 programs (for Zeeman line).

2.1. Zeeman 1 program

A flow chart of the data reduction in this program is shown in Figure 1. The solid arrows show the reduction of the original data. The dashed arrows show the same reduction, but for data derived from theoretical profiles computed with the Unno-Stepanov theory (Unno, 1956). The latter were computed using the following parameters: η_0 = line center-to-continuum absorption coefficient $=1.12$, Doppler width $\Delta\lambda_D = 42.5$ mÅ, damping constant $= 4\times 10^9$ sec^{-1} and $\beta_0/(1+\beta_0)\approx 1$, where β_0 is defined by $B(\tau)=B_0(1+\beta_0\tau)$ = source function variation with optical depth τ. These parameters were chosen such that they represent the line profile of the 6173 line as observed outside sunspots.

For a Milne-Eddington model with a linear source function and $\beta_0 \gg 1$, one obtains for zero Zeeman splitting for the line depth d: $d=\eta/(1+\eta)$, where η is the ratio of the line and continuum absorption coefficient. We made the Zeeman 1 reduction with both d and with $\eta = d/(1-d)$. The latter turned out to have some advantages so that this is the reduction which is shown in Figure 1. After the conversion of the measured line depth into η we determined first the Doppler shift $\Delta\lambda_V$. This was done by inverting the wavelength scale of one of the two circularly polarized spectra. Then the cross-correlation function was determined between the two spectra. The position of maximum cross correlation corresponds to $2\Delta\lambda_V$. Next we determined the V-Stokes parameter of the line by subtracting the two spectra (after restoration of the wavelength

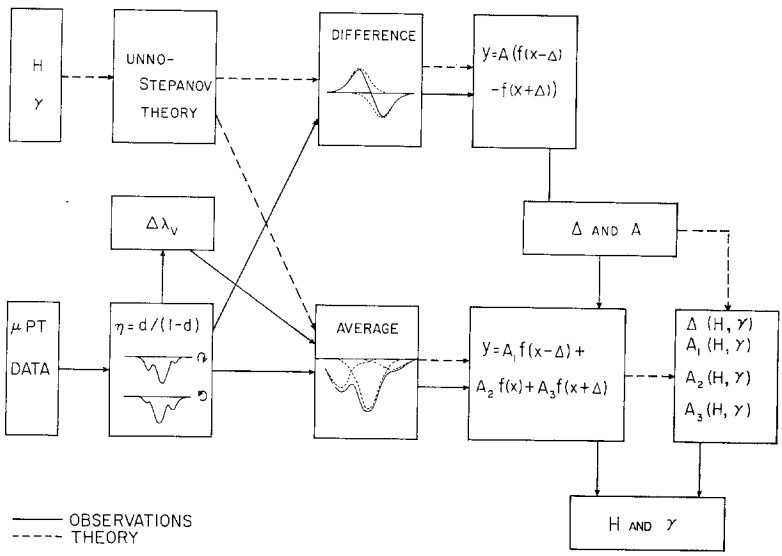

Fig. 1. Block diagram showing the reduction of the Zeeman line $\lambda 6173$ data according to Zeeman program 1.

inversion). This V-Stokes parameter (also called the difference profile) was then represented by an expression of the form $A[f(x-\Delta)-f(x+\Delta)]$, where $f(x)$ represents the line-absorption coefficient determined from the photospheric line profile, and where A and Δ are parameters which were determined by a least square fit of this equation with the data. Of primary interest here is Δ which can be expressed in a magnetic field $\hat{H}$. This $\hat{H}$ is close to the true magnetic field H. The differences between $\hat{H}$ and H are shown in Figure 2 for both the reduction with d and η. These curves were determined by applying the above procedure to the theoretical line profiles computed from the Unno-Stepanov theory. For the η approach this difference is very small ($\leqslant 1\%$) in contrast to the d approach.

Using the Δ obtained from the V-Stokes parameter we next determined the amplitude of the two σ and π components. This was done by fitting the average profile to the expression $A_1 f(x-\Delta)+A_2 f(x)+A_3 f(x+\Delta)$. From A_1, A_2 and A_3 we derived an angle $\hat{\gamma}$ such that these coefficients behave like: $A_1:A_2:A_3=(1+\cos\hat{\gamma})^2:2\sin^2\hat{\gamma}:(1-\cos\hat{\gamma})^2$ (corresponding to the Seares formula). Again the calibration of $\hat{\gamma}$ in terms of γ (true angle of the magnetic field to the line of sight), is derived from theoretical profiles computed with the Unno-Stepanov theory. Also for γ the η approach is better than the d approach. Figure 3 shows the quantities $(H-\hat{H})$ and $(\gamma-\hat{\gamma})$ as a function of $\hat{H}$ and $\hat{\gamma}$. These are the corrections which have to be applied to $\hat{H}$ and $\hat{\gamma}$ in order to get H and γ.

The reduction with the Zeeman 1 program works properly only for magnetic fields >700 gs. For smaller fields one cannot measure H and γ separately; there one can only determine $H_{\|}=H\cos\gamma$. The above-described reduction is based on the assumption that $f(x)$, or the absorption coefficient profile, does not change when going

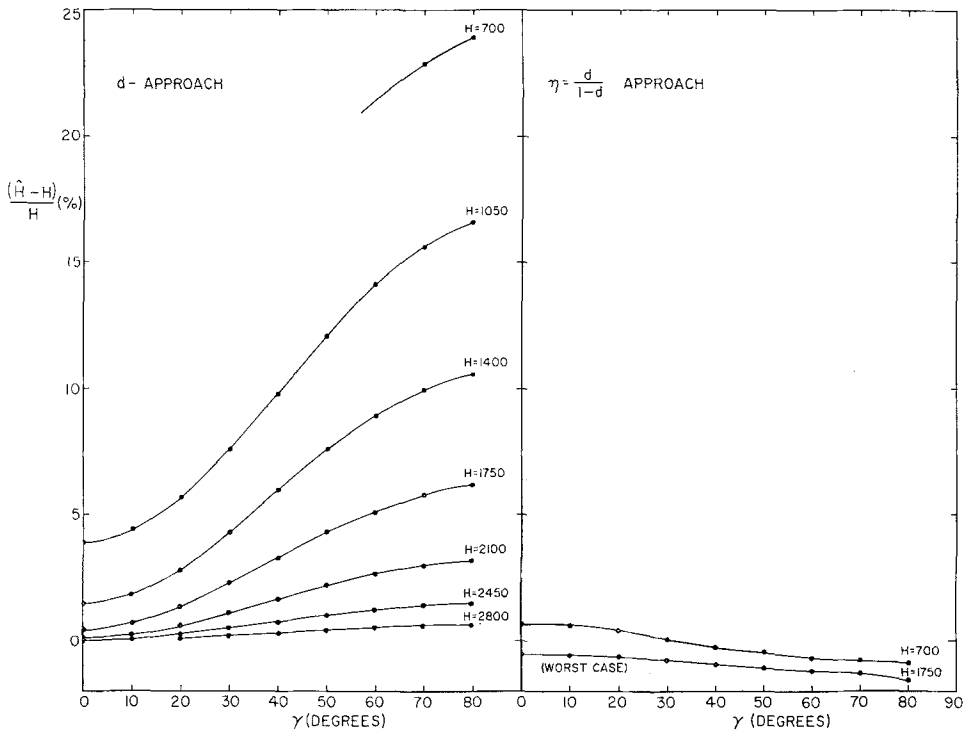

Fig. 2. Corrections to the magnetic field $\hat{H}$ as deduced from Zeeman program 1 for the d and η approach.

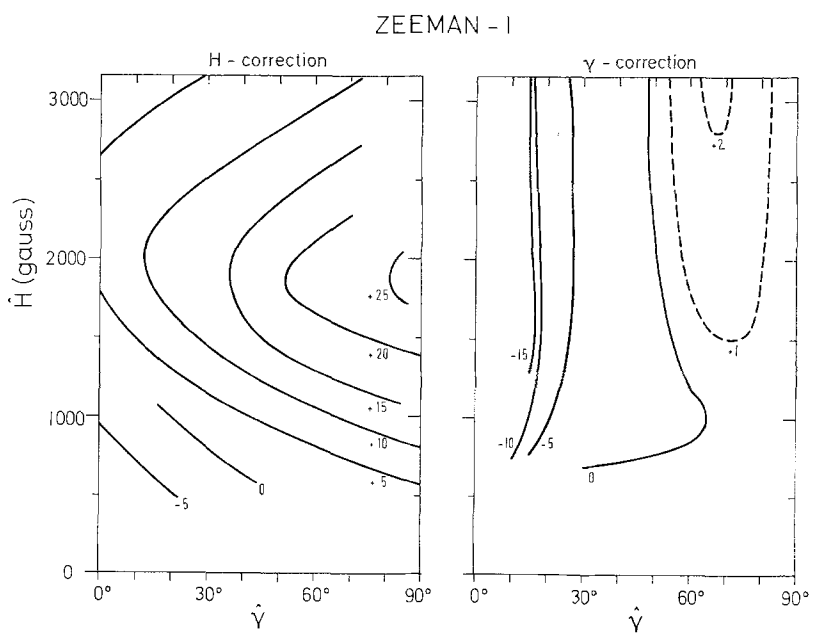

Fig. 3. Corrections to the $\hat{H}$ and $\hat{\gamma}$ for the Zeeman program 1 (corrections are in gauss and degrees, respectively)

from the photosphere into the spot and that β_0 remains still large as compared to 1. The quantity η_0, and therefore the line strength, may vary without affecting $\hat{H}$ or $\hat{\gamma}$ very much.

2.2. ZEEMAN 2 PROGRAM

The Zeeman 1 program can only be applied when instrumental polarization and retardation is absent or small. This is the case for the Sacramento Peak coronagraph but not for the coelostat telescope which also has been used for our observations. We therefore made a different reduction of the data for those days where the coelostat had been used. A block diagram of this reduction is shown in Figure 4. First we

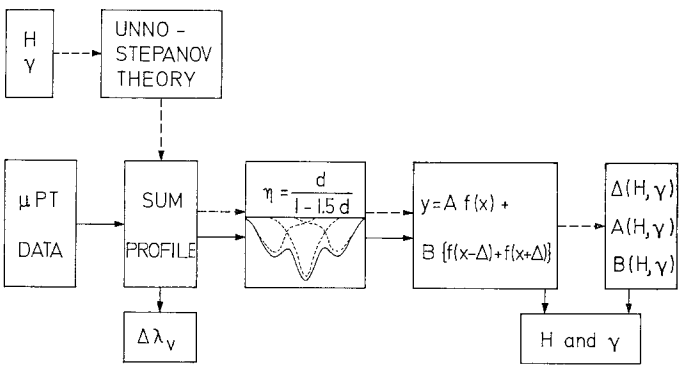

Fig. 4. Block diagram showing the reduction of the Zeeman-line $\lambda 6173$ data according to Zeeman program 2.

averaged the two profiles thereby eliminating the $\lambda/4$ plate action and the instrumental retardation. The resulting profile is identical to the one which would have been observed if no polarization optics had been present. The local change in the center of gravity of this profile is taken as the local Doppler shift. The entire line profile was expressed by least squares in a relation of the form $y = Af(x) + B\{f(x-\Delta) + f(x+\Delta)\}$. The quantity Δ represents again the magnetic field $\hat{H}$ and the ratio A/B gives $\hat{\gamma}$. A determination of η from $d/(1-d)$ is now invalid. From general considerations one obtains $\eta = d/(1-kd)$, where $1 \leqslant k \leqslant 2$. Rather arbitrarily we made the reduction with $\eta = d/(1-1.5d)$. Figure 5 shows the differences $(H-\hat{H})$ and $(\gamma-\hat{\gamma})$ as obtained from the theoretical line profiles after applying to them the Zeeman 2 program. These corrections are much larger than those for the Zeeman 1 program. Program 2 already breaks down for fields $\leqslant 1250$ gs since its application is much more sensitive to noise in the data than Program 1. Also, in this respect, the Zeeman 1 program is preferred.

In both Zeeman programs the equivalent width of the line and the continuum intensity were also determined so that for each spectral scan through the sunspot the following quantities were available: continuum intensity I_c, the Doppler shift $\Delta\lambda_V$, the magnetic field H, the relative strengths of the σ and π components ($I_{\sigma r}$, $I_{\sigma v}$, I_π), γ and the equivalent width W.

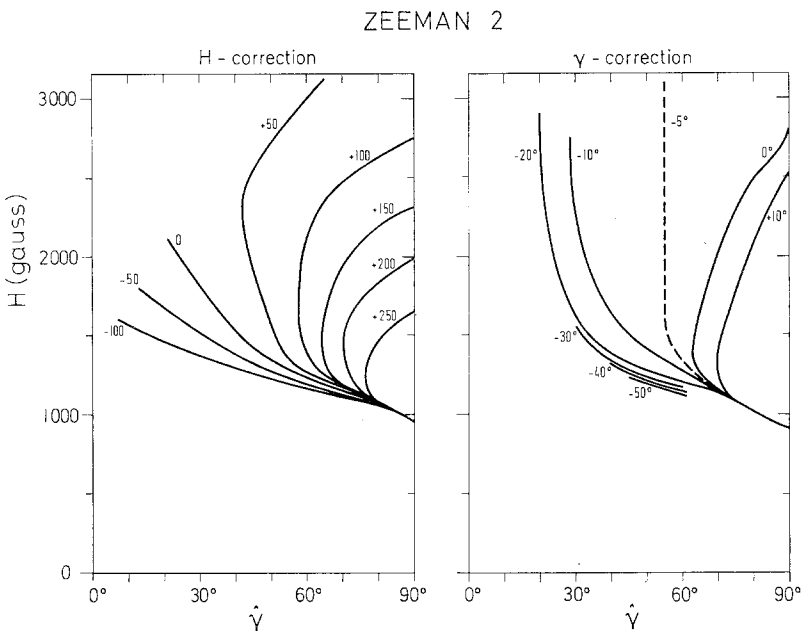

Fig. 5. Corrections to the $\hat{H}$ and $\hat{\gamma}$ for the Zeeman program 2 (corrections are in gauss and degrees, respectively).

2.3. Doppler line program

From the photometry of the line profile of the Fe line $\lambda 5576$ the following parameters were obtained by the Doppler line program:

(1) The maximum line depth d_1.

(2) The line widths at the depths $d_{.8}=0.8\,d_1$, $d_{.5}=0.5\,d_1$ and $d_{.2}=0.2\,d_1$. These widths we called $w_{.8}$, $w_{.5}$ and $w_{.2}$, respectively.

(3) The Doppler shifts $s_{.8}$, $s_{.5}$, $s_{.2}$ at these depths as well as the Doppler shift of the line center (d_1): s_1.

(4) The line asymmetry A defined by $s_x=Aw_x+B$. The quantity A was determined from the $x=.2, .5, .8$ data by least squares.

(5) The equivalent width W.

3. The Variation of the Magnetic Field across the Sunspot

In this section we will discuss the variation of H, the zenith angle ζ of the field and its vortex angle ψ with the distance ϱ from the sunspot center. Any fine structures of the field within the umbra and penumbra have been ignored. Section 5 gives a discussion of these fine structures.

The variation of H with ϱ can best be derived from the line splitting as determined with Zeeman programs 1 and 2. For the determination of the angles ζ and ψ we used two different methods. Apart from the determination directly from the Zeeman

programs (relative strengths of the σ and π components), we gave special attention to the positions in the sunspot where $H_{\|} = H \cos \gamma = 0$ (see Hale and Nicholson, 1938). These positions form a line often misleadingly called the 'neutral line'; we will refer to it as the '$H_{\|} = 0$ line'. The determination of the angle γ from the relative strengths of the π and σ components is subject to some uncertainties. For example, the ratio I_σ / I_π is affected by scattered light, by the neglected variation in line strength, by instrumental polarization, etc. These effects will all influence γ except when $\gamma = 90°$ or $H_{\|} = 0$. We therefore tend to give more weight to the result as obtained from the $H_{\|} = 0$ line investigation.

3.1. The orientation of the field from the $H_{\|} = 0$ line

In Figure 6 we show the $H_{\|} = 0$ line for different disk positions of the sunspot. The drawings of the spot have been corrected for foreshortening. The spot showed appre-

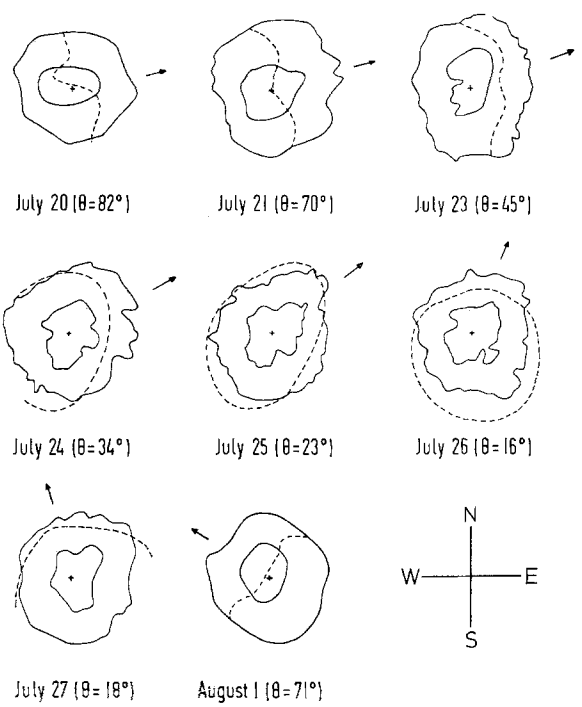

Fig. 6. The position of the $H_{\|} = 0$ line (= dashed line) for various disk positions of the spot. The arrows indicate the direction to the limb.

ciable changes from day to day and was often far from symmetric. The following reduction is based on the assumption that the field is symmetric and constant during the disk passage of the spot. The results therefore contain some uncertainty.

If one calls the position angle of the $H_{\|} = 0$ line intersections with ϱ = constant (ϱ = distance from center of spot expressed in sunspot radius) with respect to the

direction to the solar limb ϕ_1 and ϕ_2, one can show that

$$H_h/H_\varrho = \tan\theta \cos\left(\frac{\phi_1 + \phi_2}{2}\right) = \tan^{-1}\zeta \tag{1}$$

$$H_\psi/H_\varrho = \tan\left(\frac{\phi_1 - \phi_2}{2}\right). \tag{2}$$

In Equations (1) and (2) ϕ_1 and ϕ_2 are always between 0° and 180° and H_ϱ, H_h, H_ψ are the radial, vertical and tangential components of the magnetic field, respectively. Equations (1) and (2) give for all ϱ for which an intersection with the $H_{||}=0$ line occurs a value for H_h/H_ϱ and H_ψ/H_ϱ. In Table I, columns 2 and 3 list the quantity ζ and H_ψ/H_ϱ for various ϱ. The presence of a tangential component H_ψ is very doubtful. The values in Table I appear to give a small positive value for H_ψ/H_ϱ of about $+0.1$. This is in the direction which one would expect if Coriolis forces would cause the vorticity in the field. In Subsection 3.3 we will discuss the ζ behavior.

TABLE I

Variation of the magnetic field across the sunspot

ϱ	ζ[a] (°)	H_ψ/H_ϱ	ζ[b] (°)	H (gs)	dH_h/dh[c] (gs/km)	dH_h/dh[d] (gs/km)
0.0	0			2550	−0.48	−2.0
0.1	24 ± 5	0.0 ± 0.3	34 ± 4	2530	−0.47	−0.95
0.2	34 ± 5	0.0 ± 0.3	39 ± 5	2450	−0.42	−0.49
0.3	38 ± 5	0.0 ± 0.3	45 ± 5	2350	−0.37	−0.31
0.4	41 ± 5	+0.1 ± 0.3	52 ± 5	2210	−0.31	−0.20
0.5	42 ± 4	+0.1 ± 0.2	58 ± 3	2050	−0.27	−0.15
0.6	48 ± 4	+0.5 ± 0.2	67 ± 2	1900	−0.22	−0.12
0.7	58 ± 4	+0.1 ± 0.2	74 ± 3	1700	−0.16	−0.11
0.8	67 ± 4	+0.1 ± 0.2	80 ± 2	1550	−0.11	−0.09
0.9	79 ± 4	+0.1 ± 0.2	84 ± 2	1400	−0.07	−0.08
1.0	90 ± 4	+0.1 ± 0.2	88 ± 1	1250	−0.00	−0.06

[a] From neutral line.
[b] From σ to π intensity.
[c] With $\zeta = 90° - \varrho$.
[d] With ζ from neutral line (column 2).

3.2. Magnetic field from Zeeman 1 and 2 programs

For a number of spectra passing through the center of the umbra, we determined the variation of H and γ with ϱ. From γ we derived the angle ζ by assuming that $H_\psi/H_\varrho = 0$. The determination of γ is, however, very dependent on the correction for stray light which is present in the umbra. We determined this amount of stray light by measuring the intensity of the umbra in the continuum and by comparing this with the umbral intensity of the same spot as measured in the white-light images. The latter have been corrected for scattered light (Wittmann and Schröter, 1969). Typically we find for

the spectra a total of 8% stray light, of which 6% originates in front of the spectrograph (and which is therefore dispersed) and 2% originates inside the spectrograph (not dispersed).

In Figure 7 the variation of H with ϱ is shown as determined for a number of spectra taken while the spot was near the center of the solar disk. The spectra represent different cross sections through the sunspot.

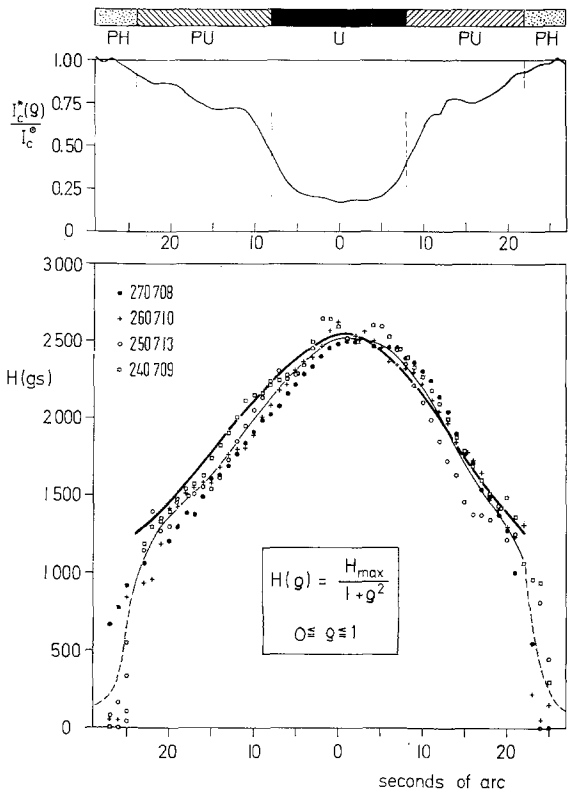

Fig. 7. The variation of the magnetic field H across the sunspot as observed from four spectra with different sunspot cross sections. The scatter of the points therefore represent partly real variations. The thin line represents the average of the H measurements. After correction, according to Figure 3, the heavy line gives the best analytic representation of $H(\varrho)/H(0)$.

The $H(\varrho)$ curve shows two interesting properties:

(a) The field decreases to 1300 gs at the photosphere-penumbra boundary, then it falls very rapidly to a very small field. Within the spot its variation is very well represented by

$$H(\varrho) = H(0)/(1 + \varrho^2). \quad (0 \leqslant \varrho \leqslant 1) \tag{3}$$

The weak magnetic fields observed outside the sunspot are caused by blurring of penumbral light into the photosphere and by magnetic knots.

(b) The field does not show any discontinuous change at the penumbral-umbral

boundary. One might have expected such a change from the Wilson effect. Later in this section, we will find a height gradient of H at this boundary of 0.4 gs/km. The Wilson effect for this spot equals 670 km (Wittmann and Schröter, 1969). This results in a field decrease of 270 gs at the umbral-penumbral boundary. The actual discontinuity is, however, less than 100 gs corresponding to less than 250 km height difference. One should remember, however, that the Wilson effect is measured in the continuum. The 6173 line is formed at a smaller optical depth where the Wilson effect consequently must be less. This agrees qualitatively with the results of Wittmann and Schröter who also find a decrease of the Wilson effect for decreasing τ.

In Figure 8 and in column 4 of Table I we show the $\zeta(\varrho)$ values. These lie systematically above those determined by means of the neutral line method. In the center of the umbra the $\zeta(\varrho)$ is definitely unequal to zero which means that the π component does not disappear (see Subsection 3.3).

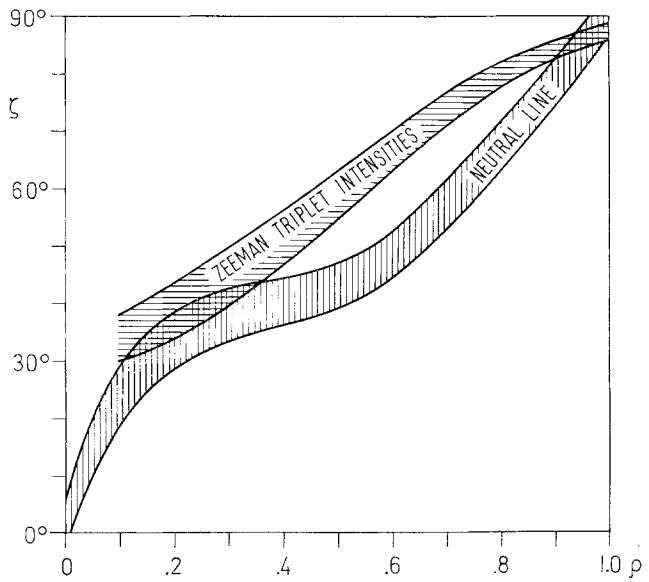

Fig. 8. Zenith angle ζ of the magnetic field as a function of ϱ. The width of the bands corresponds to one standard deviation.

From $\zeta(\varrho)$ and $H(\varrho)$ it is possible to determine the height gradient of the vertical component H_h of the magnetic field. From div $\mathbf{H}=0$ and $H_\psi=0$ it follows that $\mathrm{d}H_h/\mathrm{d}h = -\mathrm{d}H_\varrho/\mathrm{d}\varrho - H_\varrho/\varrho$. In Table I, columns 6 and 7, the values of $\mathrm{d}H_h/\mathrm{d}h$ are listed for the $H(\varrho)$ values in column 5 and for $\zeta(\varrho)=90°\,\varrho$ and $\zeta(\varrho)$ as listed in column 2, respectively. We consider the first $\zeta(\varrho)$ distribution ($=90°\,\varrho$) to be the most realistic when other observations are also considered (Subsection 3.3). In the center of the umbra the gradient equals 0.5 gs/km in the first and 2 gs/km in the second case. These values are comparable to the results of other determinations (see, e.g., Bray and Loughhead, 1964).

3.3. Discussion of the average field in a sunspot

In Figures 9 and 10 we compare our estimates of ζ and $H(\varrho)/H(0)$ with those of others. For both quantities the results obtained by the different observers vary greatly. For ζ our curve falls within the range covered by others, our $H(\varrho)/H(0)$ curve lies systematically higher. However, it resembles closely the curve published by Rayrole (1967).

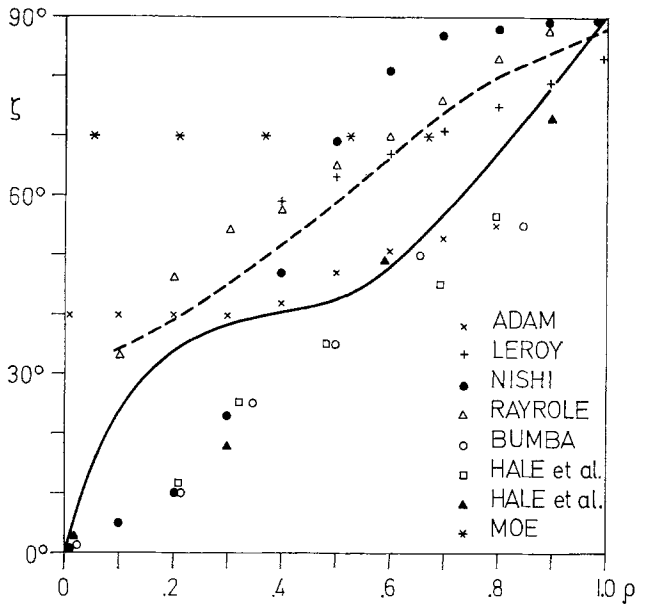

Fig. 9. Comparison of the present $\zeta(\varrho)$ observations with other results; the two symbols for Hale and Nicholson correspond to the two different methods used.

Most of the $H(\varrho)$ values represented in Figure 10 are derived from a measurement of the distance of the Zeeman-split components of the lines as seen through a compound $\lambda/4$ plate. For fields less than 1500 gs this splitting is too small to cause a separation of the σ and π components. Even for larger fields these components are only partly separated so that there still is a strong influence on the $H(\varrho)$ determination. For the fields less than 1500 gauss, one will therefore generally measure too small a field. For very small fields, the splitting as seen through the compound $\lambda/4$ plate will equal $H\cos\gamma$ instead of H. Our reduction with the Zeeman 1 and 2 programs is not influenced by these effects. We therefore believe our values of $H(\varrho)/H(0)$ to be realistic. This means that the field strength at the outer border of the penumbra still equals about 1300 gs. If the $H\cos\gamma$ values computed from our $H(\varrho)$ and $\zeta(\varrho)$ curves are compared with the other $H(\varrho)$ determination we actually find a very close agreement especially with the curve by Mattig (1952) again indicating that the normally published values refer more to the longitudinal than to the true fields.

The $\zeta(\varrho)$ curves in Figure 9 show very large differences. This may be partly due to

the fact that different spots were used, and partly due to the different methods of measuring γ and thereby ζ. If the sunspot magnetic field were homogeneous in strength and direction, one would expect the same results for all methods. The large deviations in Figure 9 may therefore be explained by inhomogeneities in the magnetic field. In particular we believe this to be the case for the differences between the two $\zeta(\varrho)$ curves as described in Subsections 3.1 and 3.2. In the center of the spot at the center of the disk we find, after correction for scattered light, the π component to be present resulting in the non-zero value for $\zeta(0)$. From $\zeta(0)=35°$ one finds for the ratio of π to σ intensity 14%. In Beckers and Schröter (1968b, 1969) we suggested an inhomo-

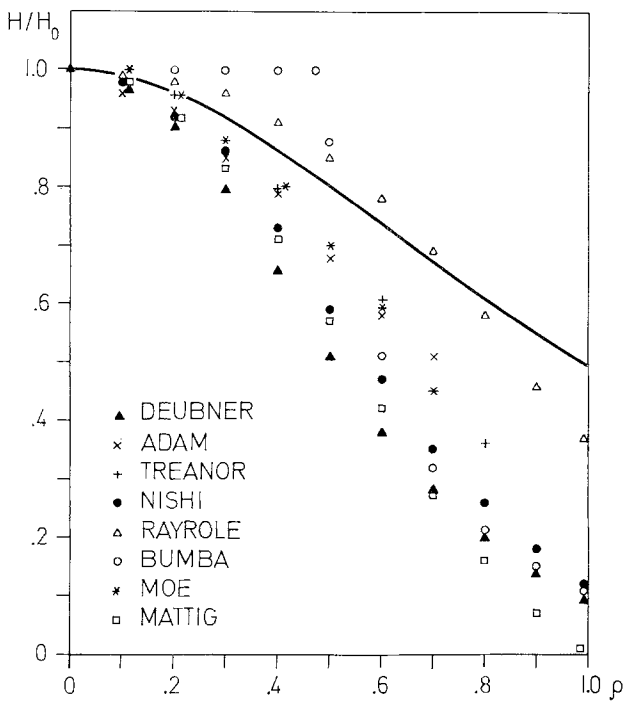

Fig. 10. Comparison of our results for $H(\varrho)/H(0)$ with other published data.

geneous model for the umbral magnetic field consisting of a field of ± 3000 gs covering most of the umbra and of a field of ∓ 300 gs associated with the umbral dots. The latter contributes only a little to the line profile but would cause an apparent π component in the center disk umbra. This model agrees with the present observations of the presence of a π component provided that the ratio of the umbral $\lambda 6173$ line coming from the 3000 gs and 300 gs regions equals 7 to 1.

It is not clear yet how all of the differences in Figure 9 could be explained in terms of fine structure of the field. A detailed observational program to study the field in one spot in all possible different ways would be of the greatest interest. It would probably result in an estimate of the magnetic field inhomogeneities.

4. Results from the Doppler Program

4.1. General

The initial aim of the Doppler-line observations was to investigate the Evershed material-flow inhomogeneities from spatial highly resolved spectra (see the conflicting suggestions concerning the inhomogeneous Evershed effect made by Schröter, 1965, and Beckers, 1966). On July 25, 26, and 27, when the spot was close to the center of the solar disk, we indeed succeeded in obtaining spectra showing strong local fluctuations of the Doppler shifts which are correlated with intensity fine structures (see Subsection 5.1). However, because these Doppler shifts represent upward and down-

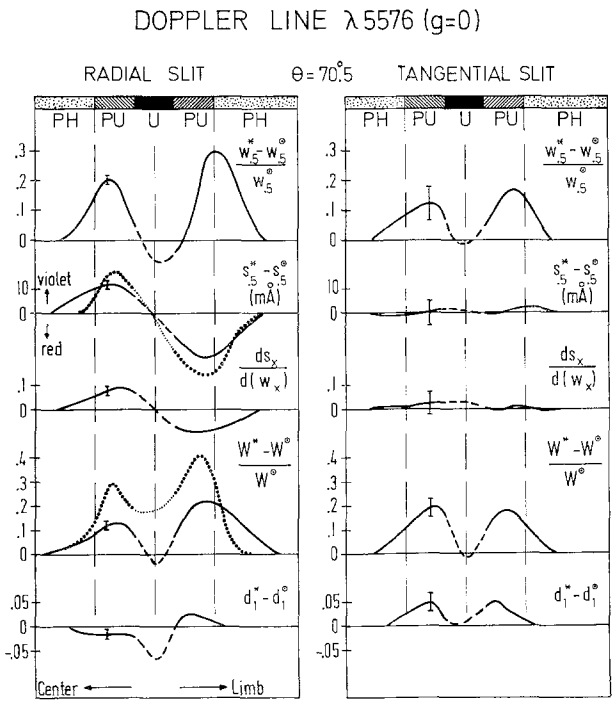

Fig. 11. Variation of the half width ($w_{.5}$), the Doppler shift at half depth ($s_{.5}$), the line asymmetry (ds/dw), the equivalent width (W) and the line depth d_1 across the sunspot. * refers to the spot, ○ to the surrounding photosphere. The dotted lines are for λ6173, the full-drawn lines for λ5576.

ward motions rather than a radial outflow, they do not refer to what one generally calls Evershed effect. On the other days, when the spot approaches the limb and the radial Evershed motion becomes dominant, the spatial resolution of our spectra is not better than that of previous observers (see Schröter, 1967). In Figure 11 we show the Evershed effect of this particular sunspot as obtained from the Doppler shift of λ5576 at $d_{.5}$ and from the shift of the entire profile of λ6173. The two curves in Figure 11 represent the average of observations made on July 21 ($\theta_{east}=70.3°$) and

August 1 ($\theta_{\text{west}}=70.7°$) and agree well with those derived by previous observers from spectra of medium or small spatial resolution. The maxima give 0.9 and 1.1 km/sec for the radial component of the Evershed effect for the Doppler and Zeeman lines, respectively. In this respect, this particular sunspot shows a radial material outflow slightly smaller than that observed by previous authors for spots of similar size (Schröter, 1967). In agreement with most other observers but in contradiction to Abetti (1932), we do not find any vorticity of the material flow (see the Doppler shift curve for the tangential slit). Figure 11 also gives the line asymmetry A of $\lambda 5576$, which shows the same behavior as the Doppler shift curves. Hence, we confirm the results of Bumba (1960), Servajean (1961), Holmes (1963), and Schröter (1965), who found the Evershed effect to consist of a line asymmetry instead of a real shift of the entire line profile.

Because of the day-to-day variation of the spatial resolution, it was difficult to study the center-to-limb variation of the Evershed effect as has been done by Schröter (1965). Therefore we decided to abandon this point of the investigation. Instead we concentrated on the following aspects:

(1) The relation between the $H_{\parallel}=0$ and $s_x=0$ line,

(2) the variation of W, $w_{.5}$ and d_1 across the spot penumbra.

4.2. The relation between the $H_{\parallel}=0$ and $s_x=0$ line

From Figure 11, and from similar drawings obtained for other disk positions of the spot, it is seen that the $s_{.5}=0$ line passes through the center of the umbra even when the $H_{\parallel}=0$ line (see Figure 6) lies well inside the penumbra. This is even the case if a correction is made for the blue shift of $\lambda 5576$ in the photosphere caused by the granular convection (≈ 0.3 km/sec). Most pronounced is this discrepancy for $60 \geqslant \theta \geqslant 40°$ where we find $H_{\parallel}=0$ near the maximum of the Evershed effect. We therefore fully confirm the observations of Semel (1967) and Rayrole (1967) who also found the magnetic 'neutral line' not to coincide with the velocity 'neutral line'. If the matter has to flow along the magnetic lines of force, one has to infer inhomogeneities in the magnetic and velocity fields which are responsible for the observed discrepancy. In the case of strong inhomogeneities in the magnetic and velocity fields, the $H_{\parallel}=0$ and $s_x=0$ lines lose their meaning.

4.3. The variation of the equivalent width, the half width and the central depth of $\lambda 5576$ across the penumbra

Figure 11 gives, as a typical example, the behavior of W, $w_{.5}$ and d_1 for a radial and tangential cross section of the spot. The most striking effect is the increase of W and $w_{.5}$ within the spot penumbra. The following effects may lead to an increase of W and $w_{.5}$:

(1) The temperature effect (change of the number of absorbing atoms).

(2) The change of model (change in the temperature stratification $\mathrm{d}B(\tau)/\mathrm{d}\tau$).

(3) The pressure effect (which changes the ionization of Fe and which mainly influences the wings of a saturated line).

(4) The effect of large-scale (Evershed) velocity inhomogeneities, or 'macroturbulence' (which results in a broadening and flattening of the line without a change of W).

(5) The effect of 'microturbulence' which results in an increase of W and $w_{.5}$ and a decrease of d_1.

(6) The effect of a W change by the magnetic field (saturation effect acting on the triplet components).

(7) The effect of temperature inhomogeneities (which result in a complicated change in W and $w_{.5}$).

The effect (6) explains most likely a part of the difference in the W increase between $\lambda 6173$ and $\lambda 5576$. Computations give for $\lambda 6173$ a maximum increase of $\approx 10\%$ in W. The excitation potential of $\lambda 5576$ (3.43 eV) is responsible for its insensitivity to temperature changes. We did not observe any change of W (5576) from center to limb nor a change of W between photosphere and spot umbra. Therefore, we can exclude the interpretation of the observed W increase in terms of effects (1) and (7). The same is valid for effect (2). All previous observations of the center-to-limb variation of the contrast penumbra photosphere (see, e.g., Wittmann and Schröter, 1969) show this contrast to be constant so that $[\mathrm{d}B(\tau)/\mathrm{d}\tau]_{\mathrm{PU}} \approx [\mathrm{d}B(\tau)/\mathrm{d}\tau]_{\mathrm{PH}}$. The Doppler line is not saturated enough in order to explain the W increase by the increase of the line wings (effect 3). The effect (4) may partly be responsible for the increase of $w_{.5}$ but certainly not for the W increase. Moreover, we observe W to increase even when the macroscopic motions are small or zero (tangential slit). Hence, this discussion provides a strong indication of an increased 'microturbulence' in the penumbra. These small-scale (< 50 km) nonthermal motions appear to be isotropic since the change in W is the same for all cross sections within the spot penumbra and at all θ positions of the spot. Since the maximum of W and $w_{.5}$ coincides with the maximum in the Evershed flow, we tend to think in terms of a microturbulence generated by the Evershed motions.

5. Fine Structure of the Magnetic and Velocity Field

From some of the spectrograms with the highest resolution (1–2 arc sec), we studied the fluctuations of various line-profile parameters on a small scale. These included the variation across penumbral filaments, across umbral dots, across a small umbral light bridge and across elongations of penumbral filaments which penetrate into the umbra.

5.1. Penumbral fine structure

To study the variation of the various parameters we made cross correlations of the quantities of interest. This was done after the running mean over 5 arc sec was subtracted including only data which lie within the penumbra. Tables IIA, B and C list the correlation coefficients for the Doppler and Zeeman data, obtained from spectra exposed when the sunspot was close to the center of the solar disk. In the present notation a blue shift corresponds to a positive line-of-sight velocity.

TABLE IIA

Cross correlation in penumbra of Doppler spectra

	$w_{.2}$	$w_{.5}$	$w_{.8}$	$s_{.2}$	$s_{.5}$	$s_{.8}$	s_1	A	W	d_1
I_c	$-.22$ $\pm.07$	$-.35$ $\pm.05$	$-.27$ $\pm.06$	$+.29$ $\pm.06$	$+.39$ $\pm.09$	$+.25$ $\pm.10$	$+.12$ $\pm.08$	$+.13$ $\pm.08$	$-.16$ $\pm.08$	$+.28$ $\pm.07$
W	–	–	–	–	–	–	–	$-.02$ $\pm.07$	–	–

TABLE IIB

Cross correlation in penumbra of Zeeman 1 spectra

	$\Delta\lambda_V$	$\lvert V_{max}\rvert$	$I_{\pi r}$	I_π	$I_{\sigma v}$	H	γ	W
I_c	$+.22$ $\pm.1$	$-.20$ $\pm.1$	$-.24$ $\pm.1$	$+.01$ $\pm.1$	$+.08$ $\pm.1$	$-.24$ $\pm.1$	$+.09$ $\pm.1$	$-.12$ $\pm.1$
$\Delta\lambda_V$	–	–	–	–	–	$-.10$ $\pm.1$	–	$-.05$ $\pm.2$
W	$-.05$ $\pm.2$	–	–	–	–	$+.08$ $\pm.1$	–	–

TABLE IIC

Cross correlation in penumbra of Zeeman 2 spectra

	$\Delta\lambda_V$	$\lvert V\rvert$	I_σ	I_π	H	γ	W
I_c	$+.31$ $\pm.12$	$-.16$ $\pm.07$	$+.11$ $\pm.12$	$-.03$ $\pm.07$	$-.37$ $\pm.09$	$-.20$ $\pm.06$	$-.05$ $\pm.12$
$\Delta\lambda_V$	–	–	–	–	$-.03$ $\pm.08$	–	$-.28$ $\pm.09$
W	$-.28$ $\pm.09$	–	–	–	$-.22$ $\pm.05$	–	–

5.1.1. *Cross Correlations for the Doppler Line*

From the correlation listed in Table IIA the following conclusions can be drawn:

(a) Bright elements have a blue shift as compared to the dark elements. Since the spot is near the center of the solar disk ($\theta \approx 16°$) and since the data which were used cover all parts of the penumbra, the line-of-sight velocity refers to upward, not out-

ward, motions. The positive correlation agrees with that found by Beckers (1969) and confirms, in this respect, the concept of penumbral filaments as convective rolls.

(b) It appears that the equivalent width W is smaller in the bright regions. This may be due to a thermal effect, a curve-of-growth effect (decrease of microturbulence) or the presence of blends which strengthen in the dark regions of the penumbra.

(c) In our notation, positive A means that the line wings have a larger blue shift than the line center. On the average, the asymmetry A is negative for the spectra which were used. The indicated positive correlation $I_c \times A$ therefore means that the line is more symmetric in the bright regions.

5.1.2. *Cross Correlations for the Zeeman Line*

In Tables IIB and C the quantity V stands for the amplitude of the V-Stokes parameter of the $\lambda 6173$ line. An increase in $|V|$ can be due to an increase of H or to a decrease of the angle γ. From Tables IIB and C we draw the following conclusions:

(a) The blue shift of the bright regions confirms the result obtained from the Doppler line.

(b) The magnetic field strength H increases in the dark regions. This appears to contradict the result published by Mattig and Mehltretter (1968). The measurements of these two authors refer, however, to $H \cos\gamma$ rather than to H and are obtained from spectra in the center side penumbra of a spot near the solar limb ($\theta \approx 45°$). Both the present measurements and those of Mattig and Mehltretter could be explained by an increase of γ and thereby an increase of ζ in the dark elements. The significant negative correlation between γ and I_c as found from the Zeeman 2 data confirms this increase in ζ in the dark regions. We therefore find a more horizontal and stronger field in the dark interfilamentary regions.

(c) The decrease of $|V|$ in bright regions is probably due to the H increase which overcompensates any increase in $\cos\gamma$.

(d) There is no clear correlation between the intensity I_c and the equivalent width W.

(e) The strength of the σ_r component ($I_{\sigma r}$), which is the strongest of the σ components, seems to increase in the dark regions of the penumbra. This is hard to explain in terms of the suggested ζ variation. This increase in the σ component strength is, however, not present in the Zeeman 2 results so that it may not be real.

5.2. Umbral fine structures

Our best spectra of the umbra often show small scale intensity fluctuations (<2 arc sec) in the continuum. Inspection of the high resolution white-light images (see Beckers and Schröter, 1968a, b) lead to three different types of structures with which these fluctuations are associated. They are:

(a) A weak light bridge which was present in the sunspot.

(b) Bright streaks which represent extensions of penumbral filaments into the umbra. A good example of this is given in Wittmann and Schröter (1969).

(c) Umbral dots themselves.

Because the spectra have a lower resolution than the white-light images, these fine

structures are of lower contrast. However, they are still visible. We examined the results of the Doppler and Zeeman programs for these features. Since the spectra were underexposed in the umbra (especially $\lambda 5576$), these results are very much noisier than the results for the photosphere and penumbra.

5.2.1. *The Weak Light Bridge*

On high resolution white-light frames, this weak light bridge appears to consist of small, bright structures very similar in size and intensity to the umbral dots (see Figure 1 in Beckers and Schröter, 1968b). In our best-resolved Zeeman line spectra crossing the light bridge, the magnetic field H is always smaller (by 200–300 gs) as compared to the surrounding umbra. After correction for scattered light, the spectra also show a significant increase of γ in the light bridge ($\Delta\gamma \geqslant 5°$). From an analysis of the Doppler line spectra, the following behavior of the line parameters was found: $W(LB) > W(U)$ (U stands for the surrounding umbra, LB for the light bridge), $d_1(LB) \lesssim d_1(U)$, $w_{.5}(LB) > w_{.5}(U)$, $s_{.5}(LB) > s_{.5}(U)$ (blue shift in the light bridge) and $A(LB) \approx A(U)$. Hence, we end up in the light bridge with a weaker, more horizontal magnetic field, with upward material motions and with a stronger, broader and flatter Doppler line $\lambda 5576$. Most likely, the local change in W, $w_{.5}$ and d_1 is due to the action of an increased 'microturbulence' in the light bridge since the Doppler line is rather insensitive to temperature changes (see Subsection 4.3).

5.2.2. *Extensions of Penumbral Filaments into the Umbra*

Several good spectra exposed at the transition region umbra-penumbra show bright streaks originating from extensions of penumbral filaments into the umbra. From 37 observed penumbral extensions, 22 show the magnetic field to be weaker as compared to the surrounding; only 2 of them show the opposite effect, and for 13 objects, any changes were buried in the noise.* For the inclination angle γ we found in the penumbral extensions $\gamma\{16, 16, 5\}$. Hence, the local increase of γ, and thereby ζ, in the penumbral extensions is less pronounced than the decrease in H. The equivalent widths of $\lambda 6173$ behave like: $W\{8, 10, 19\}$. For the local Doppler shift of $\lambda 6173$, we found $\Delta\lambda_V\{10, 12, 15\}$. The extensions therefore may have a small downward motion with respect to their surroundings. The analysis of the Doppler line $\lambda 5576$ in the extensions leads, similar to the light bridge, to a stronger, flatter and broader line profile as compared to the surrounding umbra. A very faint, if any, correlation with the line asymmetry and Doppler shift has been found ($s_{.5}\{11, 13, 13\}$) in the sense of a red shift.

For the extensions of bright penumbral filaments into the umbra, we therefore end up with a weaker and probably more horizontal magnetic field. The change of the line profile of $\lambda 5576$ can again be explained in terms of an increased 'microturbulence'. A downward material motion is indicated, but this result is rather uncertain.

* Hereafter we will express such a result by $H\{2, 13, 22\}$ where the first value gives the number of observations for which there was an increase. The second value gives the numbers of observations for which there was no effect and the last the number for which a decrease of H has been found.

5.2.3. *Umbral Dots*

Several high-quality spectra exposed on July 25, 26 and 27 show very faint and sharp streaks through the umbra. From the inspection of the best white-light frames, we found that these features have to be identified with umbral dots or with conglomerates of them. However, any possible variation of H, γ, W, I_σ, I_π, and of the line profile of $\lambda 5576$ in these streaks are buried in the large amount of noise resulting from the underexposure of the spectra in the umbra. The Doppler shift, however, shows a significant variation in the umbral dots in the sense of upward motions as compared to their surroundings. This agrees well with the observations of Beckers (1969).

Acknowledgments

The observations were made when one of us (E.H.S.) was guest investigator at the Sacramento Peak Observatory under contract AF-628-4078 with the National Center for Atmospheric Research, Boulder, Colo. A financial support was obtained from 'Deutsche Forschungsgemeinschaft, Bad Godesberg', for the reduction of the data. Mr. A. Wittmann's invaluable assistance is greatly appreciated.

References

Abetti, G.: 1932, *Publ. Obs. Arcetri* **50**, 47.
Adam, M. G.: 1967, *Monthly Notices Roy. Astron. Soc.* **136**, 71.
Beckers, J. M.: 1966, *Atti del Convegno sulle Macchie Solari*, Firenze, p. 186.
Beckers, J. M.: 1969, in *Proceedings Asilomar Conference on Plasma Instabilities in Astrophysics*, Gordon and Breach, New York.
Beckers, J. M. and Schröter, E. H.: 1968a, *Solar Phys.* **4**, 142.
Beckers, J. M. and Schröter, E. H.: 1968b, *Solar Phys.* **4**, 303.
Beckers, J. M. and Schröter, E. H.: 1968c, in *Structure and Development of Solar Active Regions.* IAU Symposium No. 35 (ed. by K. O. Kiepenheuer), Reidel, Dordrecht, p. 178.
Beckers, J. M. and Schröter, E. H.: 1969, *Solar Phys.* **7**, 22.
Bray, R. J. and Loughhead, R. E.: 1964, *Sunspots* (International Astrophysics Series, 7), Chapman and Hall, London.
Bumba, V.: 1960, *Izv. Krymsk. Astrofiz. Observ.* **23**, 212.
Deubner, L.: 1969, *Solar Phys.* **7**, 87.
Hale, G. E. and Nicholson, S. B.: 1938, *Publ. Carnegie Inst. No. 498.*
Holmes, J.: 1963, *Monthly Notices Roy. Astron. Soc.* **126**, 155.
Leroy, J. L.: 1962, *Ann. Astrophys.* **25**, 127.
Mattig, W.: 1952, *Z. Astrophys.* **31**, 273.
Mattig, W. and Mehltretter, J. P.: 1968, in *Structure and Development of Solar Active Regions.* IAU Symposium No. 35 (ed. by K. O. Kiepenheuer), Reidel, Dordrecht, p. 187.
Moe, O. K.: 1968, in *Structure and Development of Solar Active Regions.* IAU Symposium No. 35 (ed. by K. O. Kiepenheuer), Reidel, Dordrecht, p. 202.
Nishi, K.: 1962, *Publ. Astron. Soc. Japan* **14**, 325.
Rayrole, J.: 1967, *Ann. Astrophys.* **30**, 257.
Schröter, E. H.: 1965, *Z. Astrophys.* **62**, 256.
Schröter, E. H.: 1967, *Solar Physics* (ed. by J. H. Xanthakis), Wiley, New York, p. 325.
Semel, M.: 1967, *Ann. Astrophys.* **30**, 513.
Servajean, R.: 1961, *Ann. Astrophys.* **24**, 1.
Treanor, P. J.: 1960, *Monthly Notices Roy. Astron. Soc.* **120**, 412.

Unno, W.: 1956, *Publ. Astron. Soc. Japan* **8**, 108.
Wilson, P. R. and McIntosh, P. S.: 1969, in preparation.
Wittmann, A.: 1968, *Sterne und Weltraum* **7**, 268.
Wittmann, A. and Schröter, E. H.: 1969, *Solar Phys.* **10**, 357.